


 Very Important Paper


 Special Collection

# Complex pBAE Nanoparticle Cell Trafficking: Tracking Both Position and Composition Using Super Resolution Microscopy

 Roger Riera,<sup>[a]</sup> Jana Tauler,<sup>[a, b]</sup> Natàlia Feiner-Gracia,<sup>[a]</sup> Salvador Borrós,<sup>[b]</sup> Cristina Fornaguera,<sup>\*[b]</sup> and Lorenzo Albertazzi<sup>\*[a, c]</sup>

Nanomedicine emerged some decades ago with the hope to be the solution for most unmet medical needs. However, tracking materials at nanoscale is challenging to their reduced size, below the resolution limit of most conventional techniques. In this context, we propose the use of direct stochastic optical reconstruction microscopy (dSTORM) to study time stability and cell trafficking after transfection of oligopeptide end-modified poly( $\beta$ -aminoester) (OM-pBAE) nanoparticles. We selected different combinations of cationic end oligopeptides (arginine – R;

histidine – H; and lysine – K) among polymer libraries, since the oligopeptide combination demonstrated to be useful for different applications, such as vaccination and gene silencing. We demonstrate that their time evolution as well as their cell uptake and trafficking are dependent on the oligopeptide. This study opens the pave to broad mechanistic studies at nanoscale that could enable a rational selection of specific pBAE nanoparticles composition after determining their stability and cell trafficking.

## Introduction

Nanomedicine appeared some decades ago as a game changer technology that should be able to overcome all the barriers that conventional medicines have. The term nanomedicine refers to nanosized engineered materials, including organic, inorganic and hybrid formulations for medical applications.<sup>[1]</sup> It does not only include therapeutics, but also diagnostic and theragnostic applications.<sup>[2–4]</sup> To achieve these envisaged purposes, nanomedicines need to incorporate an active principle. Among different kinds of macromolecules, nucleic acids are gaining importance for genetic and infectious diseases and cancer therapies. mRNA vaccines for SARS-CoV-2 infection


prophylaxis are probably the most striking example nowadays.<sup>[5,6]</sup> In fact, it was not until the appearance of nanomedicine that the use of nucleic acids as therapeutics became a reality, since, being labile compounds, they need a protective carrier to be delivered intact in their target cells before being degraded by nucleases in physiological fluids/tissues.<sup>[7]</sup> First attempts of nucleic acid delivery were focused on gene therapy using viral vectors. However, scientists early realized the unsolvable drawbacks that viruses pose regarding safety issues, together with expensive production costs and limited loading/short genes encoding capacity. Therefore, non-viral vectors rapidly gained importance thanks to their possibility to encapsulate longer nucleic acids, at higher doses, being produced in an easy and affordable to scale up technology, and thanks to their fine tailoring capacity; in addition of safety improvement.<sup>[8,9]</sup>


A wide variety of materials can be used as non-viral gene delivery systems, being polymers and lipids the most important. In our group, we designed a library of oligopeptide end-modified poly( $\beta$ -aminoesters) (OM-pBAE), polymers synthesized through an easy two-step Michael addition reaction, previously demonstrated to be non-toxic and biodegradable.<sup>[10,11]</sup> Having amines in their structure, they can easily complex different kinds of nucleic acids through electrostatic interactions and form small nanometric particles (polyplexes). These nanoparticles transfect cells with an efficiency markedly higher than commercial vectors, without producing any toxicity, both in vitro and in vivo.<sup>[10–13]</sup> In addition, the use of different combinations of end-modified oligopeptides, as well as the addition of added functionalities in the lateral chains, gives the resulting nanoparticles particular properties. For example, the combination of 60% of lysine, required for the interaction with plasmatic membranes, with 40% of histidine, required for endosomal escape, end modification demonstrated a selective


[a] R. Riera, J. Tauler, Dr. N. Feiner-Gracia, Dr. L. Albertazzi  
 Department of Biomedical Engineering  
 Institute for Complex Molecular Systems (ICMS)  
 Eindhoven University of Technology  
 De Zaale, Eindhoven 5612 AZ (The Netherlands)  
 E-mail: l.albertazzi@tue.nl

[b] J. Tauler, Prof. S. Borrós, Dr. C. Fornaguera  
 Grup d'Enginyeria de Materials (GEMAT)  
 Institut Químic de Sarrià  
 Universitat Ramon Llull  
 Via Augusta, 390, 08017 Barcelona (Spain)  
 E-mail: cristina.fornaguera@iqs.url.edu

[c] Dr. L. Albertazzi  
 Nanoscopy for Nanomedicine  
 Institute for Bioengineering of Catalonia  
 Carrer de Baldri Reixac, 10, 12, 08028 Barcelona (Spain)

 Supporting information for this article is available on the WWW under <https://doi.org/10.1002/cmdc.202100633>

 This article belongs to the Special Collection "Nanomedicine: Drug Delivery and Nanodrugs".

 © 2022 The Authors. ChemMedChem published by Wiley-VCH GmbH. This is an open access article under the terms of the Creative Commons Attribution Non-Commercial License, which permits use, distribution and reproduction in any medium, provided the original work is properly cited and is not used for commercial purposes.

transfection of dendritic cells, which is advantageous for vaccination purposes;<sup>[7]</sup> while the only use of arginine end-modified polymers, including PEG moieties allowed for an improved tumor accumulation<sup>[14]</sup> and VHPK-peptide functionalization was required for endothelial cells targeting.<sup>[15]</sup> The possibility to mix and match different polymers with different functions is a great advantage of nanomedicine as it allows the formulation of materials with tuned properties. However, at the same time this poses a challenge towards the understanding and rational design of such materials as this extend the complexity of the materials and makes very difficult the study of their behavior.

Indeed, despite their promising applications, OM-pBAE nanoparticles have not yet reached clinical steps, which could be attributed to the lack of mechanistic studies describing their interaction with biological components after injection. Although their efficacy has been demonstrated broadly, their stability, safe interaction and degradation once in contact with cells has not yet been demonstrated. For this reason, more detailed knowledge on polyplexes stability and cell interaction are required. In fact, performing these types of studies at nanoscale is quite difficult, due to small nanometric sizes, below the limit of resolution of most traditional imaging techniques.<sup>[16]</sup> Conventional optical microscopes do not allow the study of particles structure and trafficking inside cells due to their spatial resolution limited by light diffraction in the range of few hundreds of nanometers.<sup>[16–20]</sup>

Luckily, some years ago, super resolution microscopy techniques were developed with the specific objective to go lower than the optical resolution. They are a powerful tool that enables to go a step further and study the structural properties of nanoparticles as well as their interaction with cells by obtaining high resolution images of nanosystems. In a previous study, we already demonstrated the possibility to use direct stochastic optical reconstruction microscopy (dSTORM) to visualize and quantify the two components of our OM-pBAE nanoparticles: the polymer and the plasmid encapsulated.<sup>[16]</sup> Following this first study that worked as the proof-of-concept of the suitability of the technique to study pBAE nanoparticles, in here, we aim to study the dynamic supramolecular structure (polyplex) and stability of OM-pBAE multicomponent particles composed by two combined polymers and pDNA as model oligonucleotide, both, in dispersion and during cell trafficking,

including decomplexation state, heterogeneity between the different oligopeptide combinations and nuclear entrance by using dSTORM on OM-pBAE nanoparticles labelled by two colors. This knowledge will enable us to better understand the role of each end-modified oligonucleotide into the polymer mixture and thus rationally select and re-design the most convenient oligopeptide combination depending on the specific nanoparticle intended use.

## Results and Discussion

### Polyplexes labelling and imaging on glass

In this work we are going to study different pBAE compositions (see Figure S1, polymer structure) and their behavior inside COS-7 cells. The polymers of choice are polymers terminated with arginine (R), lysine (K) and histidine (H) end-modified pBAEs that are combined to obtain better transfection as shown in the literature.<sup>[7,10,11]</sup> Specifically, we prepared the following combinations: RH (60/40 ratio), KH (60/40 ratio) and RK (50/50 ratio).

In order to track these mixtures in cells (2 polymers and DNA) we devise a labeling strategy for super-resolution imaging based on 2-color STORM using cy3 and cy5 dyes<sup>[16]</sup> (Figure 1a and b). Briefly, DNA is always labeled with Cy3 to identify and localize polyplexes and one of the two polymers is labeled with Cy5. These leads to multiple samples changing in polyplex composition and labeling (see Table 1).

The first step into studying these polyplexes with STORM is to achieve the right labelling percentage in order to obtain accurate single-molecule images. Since we were mixing polymers at around 1:1 ratio, we doubled the labelling density to 2% of polymers molecules in comparison to previous protocol used with single polymer polyplex, to achieve similar number of localizations per polyplex. Polyplexes were snap frozen and lyophilized after preparation, as described in the materials and methods section, to preserve them and prolong their shelf life. Polyplexes were later resuspended before usage. Firstly, we imaged them in vitro on a glass slide to corroborate our labelling strategy and their stability after lyophilization. As it is clearly demonstrated in Figure 1c–e, we were able to label either of the polymers in the pBAE mixture, simultaneously to

**Table 1.** Polyplex mixture formulations and labelling strategies.

Nanoparticle type	Given name	Polymers combination	Labelling
KH	KH*/pDNA*	60% K	Cy3:pGFP
		40% H	Cy5:H
KH	K*/pDNA*	60% K	Cy3:pGFP
		40% H	Cy5:K
RH	RH*/pDNA*	60% R	Cy3:pGFP
		40% H	Cy5:H
RH	R*/pDNA*	60% R	Cy3:pGFP
		40% H	Cy5:R
RK	R*/pDNA*	50% R	Cy3:pGFP
		50% K	Cy5:R
RK	RK*/pDNA*	50% R	Cy3:pGFP
		50% K	Cy5:K

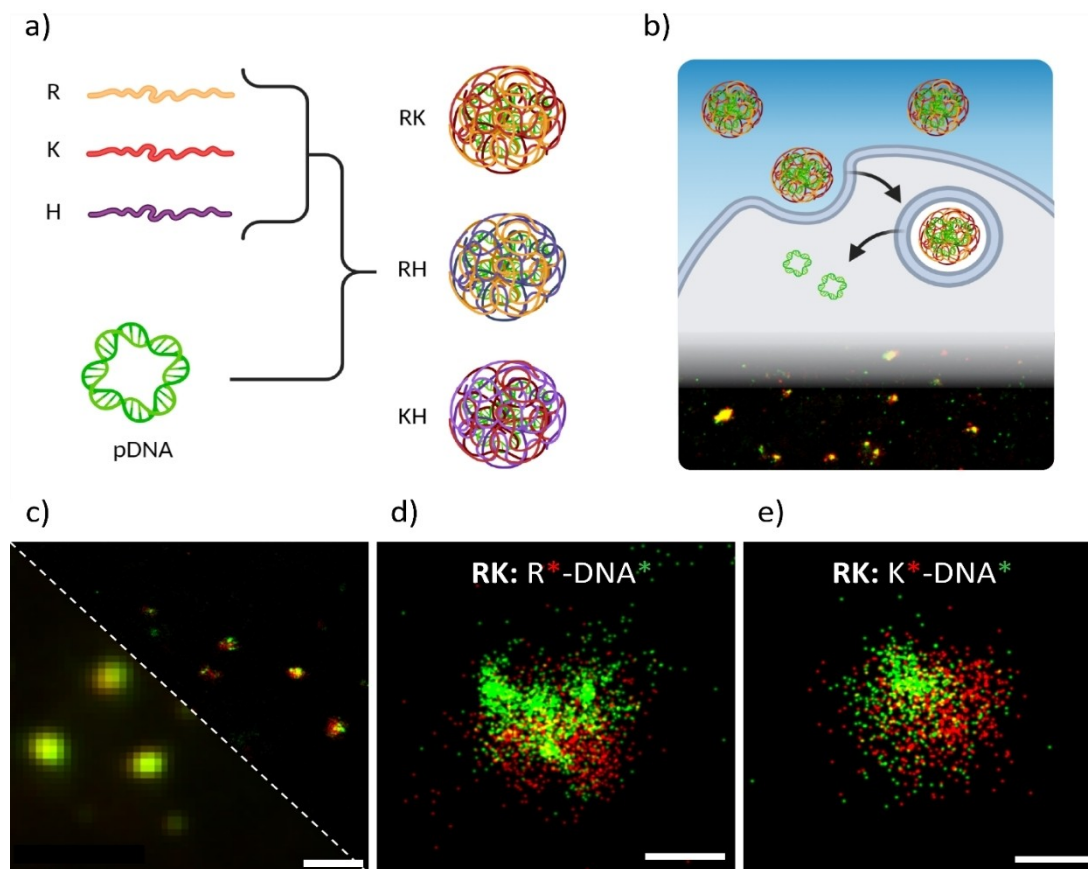


**Figure 1.** Polyplex formulation and STORM imaging. a) Polyplex formulation consists on combining pDNA with a mixture of two of arginine (R), lysine (K) or histidine (H) polymers. b) Schematic representation of polyplex cellular trafficking and STORM imaging. c) STORM images of polyplexes on a glass show the increased resolution compared to the conventional low-resolution TIRF image. d-e) STORM images of RK polyplexes - d) labelling polymer R and e) labelling polymer K - on a glass slide show the separate labelling strategy of R and K polymers. Scale bars: 1  $\mu\text{m}$  (c), 200 nm (d-e).

the plasmid labelling, and thus, we confirmed nanoparticles maintained their structure after lyophilization, using the lyophilization method we previously set up.<sup>[21]</sup>

### Polyplexes imaging and quantification in cells

A pulse-chase experiment was designed where cells were incubated with freshly resuspended labeled polyplexes for 30 minutes, before they were washed and fixed at various time points. This way, unbound polyplexes are washed away and we can follow the trafficking of the early internalized polyplexes, as both polymer and DNA contain amines that can be fixed preserving the structure of the polyplex. Multiple cells were imaged with STORM to reveal the position and complexation state of polyplexes. Basically, the amount of Cy5-labeled polymer around the DNA signal is quantified over time to assess the decrease of DNA-bound polymers due to decomplexation. To quantify the stability of polyplexes and obtain a general view of the heterogeneity of the sample, we analyzed the images with a custom Matlab script described in Feiner-Gracia et al.<sup>[22]</sup> Briefly, a mean-shift clustering algorithm is used to cluster the single-molecule localizations produced by the Cy3-

labelled pDNA. This is done in order to objectively identify the polyplexes and track the cargo along its way into the cell. Some filters are applied to discriminate aggregates and only count isolated polyplexes. Then, the localizations produced by the Cy5-labelled polymer around the pDNA cluster are counted (for a detailed description check the Experimental Section).

Figure 2 shows a representative image of cells transfected with the different polyplex formulations at first and last time points. Time points in between are shown in Figure S2. We observe all formulations are successfully internalized into the cells after the pulse of 30 minutes. At the beginning, polyplexes are found close to the membrane and start to travel through the cell cytoplasm. After 12 h incubation we find polyplexes mostly on the perinuclear area, where organelles such as ER, lysosomes and Golgi are located, as can be observed by the transmission images of cells. We also observed some of the polyplexes form large aggregates, specially KH. These bigger aggregates seem to be internalized and processed slowly and they are still observable after 12 h while individual polyplexes are rapidly disassembled.

We quantified the amount of pDNA and polymers on polyplexes over time with the previously mentioned script and plotted the results on Figure 3. An example of the distributions

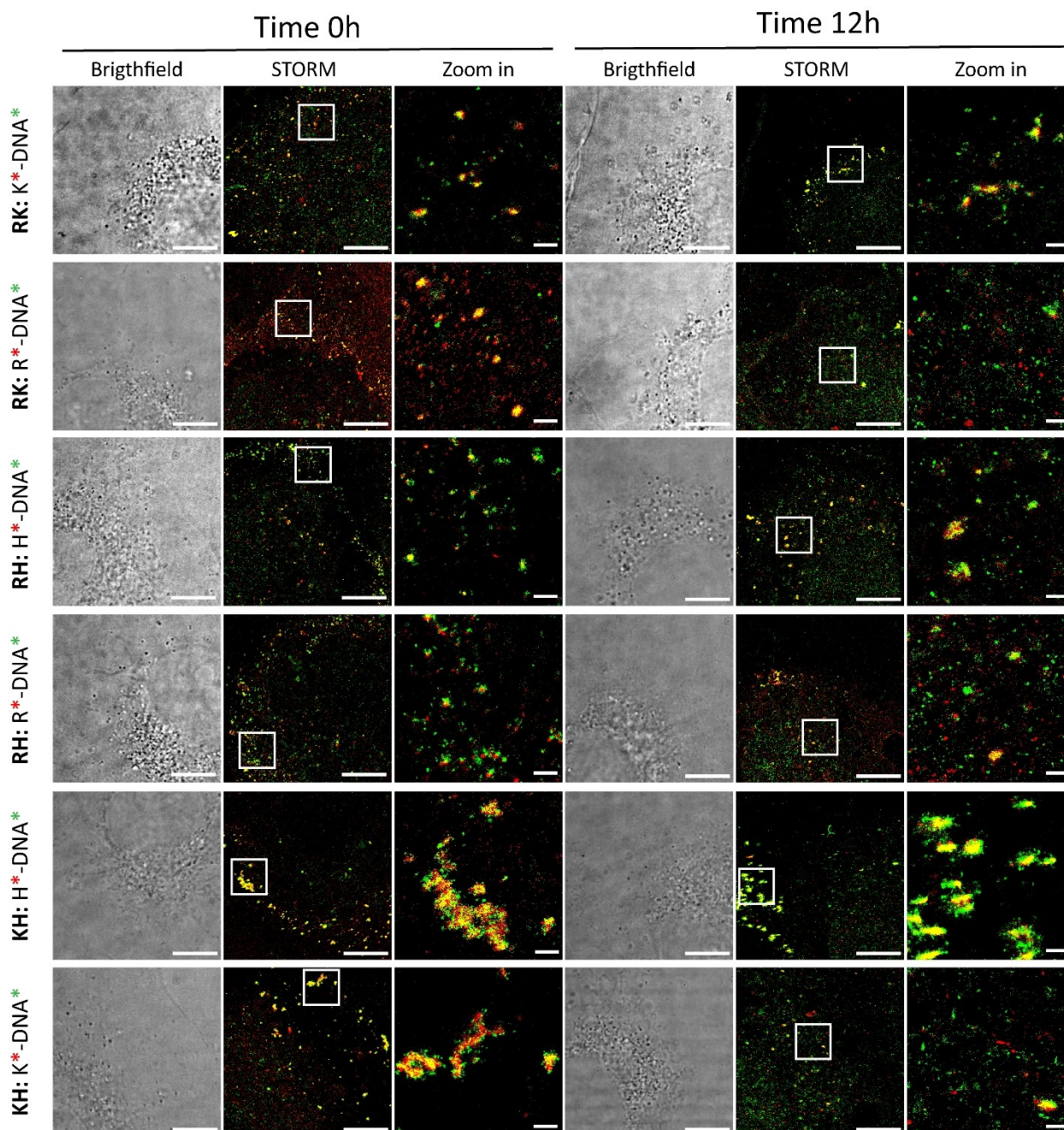


**Figure 2.** STORM images of time evolution of polyplexes inside the cell. Labelling corresponds to the polymer (red) and the pDNA (green). Each image corresponds to an individual cell. White square on STORM images is zoomed on the images on the right. Scale bars on brightfield and STORM images are 5  $\mu\text{m}$  and on zoom ins 500 nm.

of pDNA and K polymer (KH polyplex) between first and last time points are shown in Figure 3. The rest of the distributions are plotted in the Supporting Information (Figure S3-5). The main observable trend is that polymer localizations rapidly decrease over time while pDNA only decreases slightly. This is in agreement with the decomplexation of polymers from a single DNA-labeled strand. To better compare these results, we plotted the median value of these distributions on Figure 4 (see other polyplexes in Figure S6 and S7). Interestingly, each

polymer mixture behaves differently. Firstly, RH polyplexes consist of both polymers at a proportion (calculated from the median counts of each polymer) comparable to the initial polymer mixture (60%R/40%H) and both polymers decrease at a similar rate. However, KH and RK polyplexes do not follow the initial polymer mixture since the former incorporates more lysine polymer, and the later mostly consists of arginine pBAE. This is an important finding as polymer composition on polyplexes is not as straightforward as mixture of polymers.

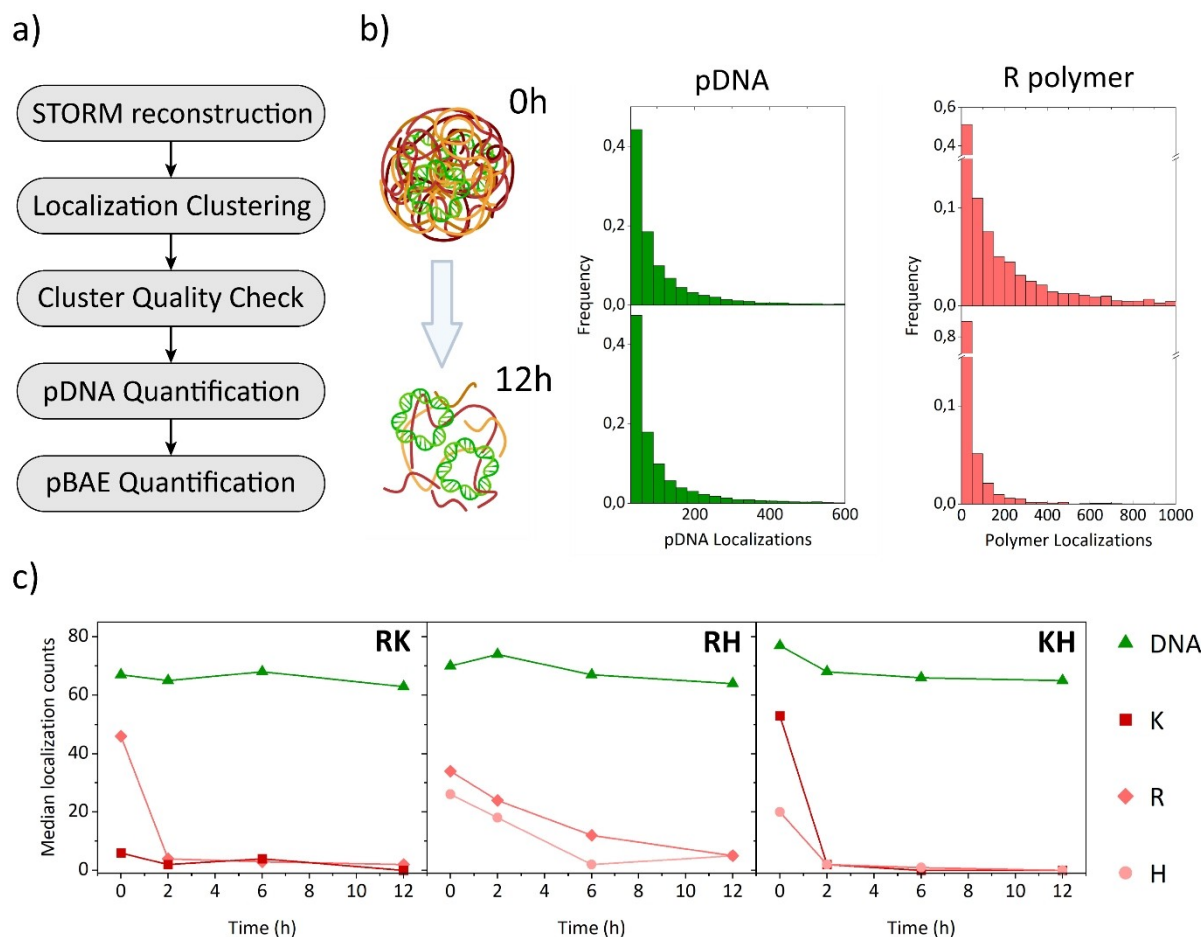


**Figure 3.** Polyplex decomplexation quantification. a) Analysis workflow of polyplex decomplexation quantification. A detailed description of the analysis procedure can be found on the Experimental section b) pDNA and pBAE (R) localizations of RH polyplexes at 0 (top) and 12 hours (bottom). c) Median values of pDNA (green triangle), K (strong red square), R (red rhombus) and H (light red circle) polymer of RK, RH and KH polyplexes. The distribution of each individual time point can be found on Figures S3–5. Frequencies of each polyplex ratios between polymer and pDNA localizations detailed in Figure 4 and Figures S6–7.

Nevertheless, the analysis only selects isolated polyplexes and does not take the clusters into account.

## Discussion

The configuration of the end-modified pBAE polyplexes have a crucial role in transfection efficiency. However, it is important to notice that what goes into the mixture during formulation is not what comes out in the polyplex. Polymers can be differentially incorporated and can have different decomplexation rates inside cells.

In this work, we started by devising the required labelling procedure using STORM microscopy as the measurement technique, which was further verified *in vitro* (Figure 1). Thus, we could determine the amount of the two polymers involved in space and time (Figure 2). Interestingly, not all internalized polyplexes followed the expected polymer mixture (Figure 3). On one hand, RH polyplexes displayed a similar ratio to the mixture of polymers used to prepare it, 56% R and 44% H from

the expected 60% R and 40% H. On the other hand, KH and RK differed from the expected mixtures. KH showed a ratio of 72% K and 28% H from the 60% K and 40% H mixture, and RK had an 88% R and 12% K ratio from the 50% R and 50% K. This must be taken into consideration since these are the real polymer mixtures and would define how the polyplexes behave inside the cell.

Polyplexes have to deliver its cargo intact for it to reach the nucleus, however, the behavior they have to follow in order achieve that is not trivial. From the three polyplexes in this study, RH show a slower decomplexation than KH and RK, in which DNA is completely released after 2 h (Figure 3). Timing the right moment for delivery could be complicated since it may depend on cell division state, since it is known that cell division is the key moment to get the DNA cargo inside the nucleus, especially when there is no nuclear targeting signal.<sup>[23–25]</sup> Therefore, having a slower decomplexing polyplex could release free DNA available to go to the nucleus during a longer period of time, therefore increasing the chance of transfection. We do not observe an increase transfection

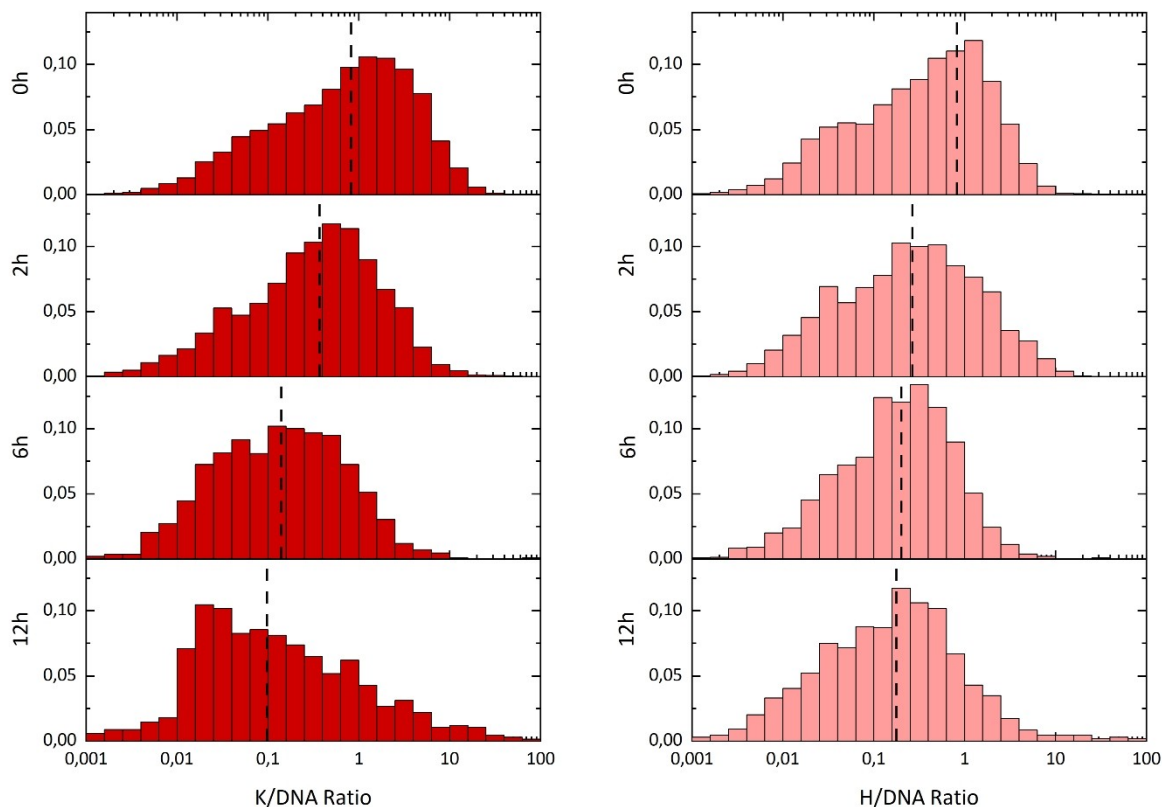


**Figure 4.** Frequencies of single KH polyplex ratios between polymer and pDNA localizations. Dashed line represents median value of the distribution.

efficiency of RH versus RK or KH (Table S1), which indicates there may be other factors that comes into play. In previous work, we demonstrated a cell-type dependence on the transfection efficiency as a function of the polymer used. Nevertheless, in here, for COS-7 cells and using the above mentioned combinations of C6 generation polymers, no significant differences were found.<sup>[11]</sup> Certainly, the location of the delivered DNA is also crucial to reach the nucleus. If polyplexes are not able to escape the endolysosomal pathway they would either be degraded or directly recycled out of the cell. Interestingly, we observe polyplexes are located in the perinuclear area after 12 h, which is known to be a prerequisite for nuclear entry of polyplexes without a nuclear tag.<sup>[23–25]</sup> Therefore, nuclear internalization would be heavily dependent on cell division, although, the complexation state at that point may be important since bigger molecules would not make it into the nucleus.<sup>[26]</sup> In our previous work,<sup>[16]</sup> we already found that DNA molecules that make it into the nucleus were naked (without polymer). However, we cannot rule out the function of bigger polyplex aggregates, since they may degrade slower and release DNA molecules in a broader range of time, allowing for a greater chance of matching the cell division process.

## Conclusion

We applied 2-colour STORM to study the stability and complexation state of pBAE polyplexes in cells. In our previous work<sup>[16]</sup> we demonstrated the validity of STORM to quantitatively study the trafficking of polyplexes, and here we expanded it to study different polymer mixtures. Interestingly, STORM revealed that the polymer mixture of polyplexes was not the one expected from ratio of polymer used in formulation. The different polymers have different affinities for the negatively charged DNA and may compete to form the polyplexes. Furthermore, we studied the decomplexation of these polyplexes over time inside the cells. Interestingly, we observe RH decomplexation is slower than RK and KH mixtures. However, KH tend to form aggregates that remain for longer time in the cell. Overall, the data presented in this work helps to give a more comprehensive understanding of the structure-function relationship of pBAE polyplexes.

## Experimental Section

**Materials:** Paraformaldehyde (PFA), glucose-oxidase from *Aspergillus niger*, cysteamine (MEA), catalase from bovine liver, glucose, sucrose, sodium acetate, HEPES and phosphate-buffered saline were purchased from Sigma-Aldrich®. Fetal Bovine Serum (FBS),

Dulbecco's modified Eagle's medium (DMEM), glutamine, penicillin and streptomycin were obtained from Gibco®. Plasmid pMAX-GFP (plasmid DNA - pDNA) (3486 bp) was produced and purified from *E. coli* and labelled with Cy3 Label IT® Tracker™ Intracellular Nucleic Acid Localization Kit from Mirus Biotech, following supplier protocol. Labelling density was adjusted to 10 dye molecules per pDNA. This was determined from the ratio of Cy3 and DNA concentrations measured in Tecan Infinite 200 Pro instrument (Tecan, Barcelona, Spain).

Arginine (R), lysine (K) and histidine (H) end-modified poly( $\beta$ -aminoester) polymers were synthesized following a two-step procedure described in the literature.<sup>[7,10,11]</sup> In brief, first, an acrylate-terminated polymer, including hexylamines in the lateral chain, C6 polymer, was synthesized by addition reaction of primary amines with diacrylates. Finally, pBAE was obtained by end-capping modification of the resulting acrylate-terminated polymer with R, H or K, named as C6-CR3, C6-CK3 and C6-CH3 or simply, R, K and H on the following. Polymer was later labelled with Cy5 at a 1 dye per pBAE molecule ratio.

Polyplexes formation and characterization: OM-pBAE nanoparticles, polyplexes, were formed by electrostatic interaction between anionic pDNA and cationic polymers, following the exact method we described before.<sup>[16]</sup> The following polymer combinations were used here: 1) RH, which refers to 60% R+40% H; 2) KH, which refers to 60% K+40% H; and 3) RK, which refers to 50% R+50% K. For optimal dSTORM imaging, polyplexes were prepared using 1% Cy5 labelled pBAE and 25% Cy3 labelled pDNA. For nuclear entry studies, polyplexes were prepared with all pDNA molecules labelled. Their characterization consisted on determining hydrodynamic size (nm) and polydispersity index (PDI), by dynamic light scattering, and their transfection efficiency in Cos-7 cells, by flow cytometry.

Polyplexes preparation for dSTORM imaging of free nanoparticles: As we described before in more detail,<sup>[16]</sup> around 35 mL of freshly resuspended nanoparticles, diluted 1/100 in PBS were added in the flow chamber and cleaned after 10 minutes to remove excess unbound polyplexes. Before imaging, dSTORM buffer was added.

In vitro samples preparation for dSTORM imaging: COS-7 cells (ATCC® CRL-1651™) were cultured in DMEM media containing 10% FBS, 2 mM L-glutamine, 100 units/mL penicillin and 100  $\mu$ g/mL streptomycin. Cells were seeded at a density of 30.000 cells/well in 400  $\mu$ L of media in an 8-well Nunc™ Lab-Tek™ (Thermo Fisher Scientific®) and let grown overnight at 37 °C and 5% CO<sub>2</sub>, to reach 70–90% confluence. As described in detail before,<sup>[16]</sup> nanoparticles were incubated with cells in complete media for different time studies, fixed with paraformaldehyde at the end of the study time and incubated with dSTORM buffer for visualization purposes.

Image acquisition and data analysis: Images were acquired in a Nanoimager® (ONI, Oxford) using the NimOS software. Cy5-labelled pBAE was imaged with a 640 nm laser (190 mW), Cy3-labelled pDNA was imaged with a 532 nm laser (300 mW). The sample was illuminated using a total internal reflection fluorescence (TIRF) alignment system and the z-level was kept constant using the build-in perfect focus system. Fluorescence was recorded using ONI 100 $\times$ , 1.49 NA oil immersion objective and passed through a quad-band pass dichroic filter. Images were acquired onto a 425 $\times$ 518 pixel region (pixel size 0.117  $\mu$ m) at 10 ms integration time for dSTORM imaging. For dSTORM images, two colour images were obtained simultaneously by means of a beam splitter: 21.000 frames were acquired and the first 1.000 were discarded. Individual point-spread function (PSF) were fitted with a 2D gaussian function on the NimOS software to obtain the reconstructed dSTORM image. A minimum photons threshold was set to 300. To objectively

identify and quantify polyplexes, the list of localizations of the dSTORM images were exported and analysed in a Matlab script previously described by Feiner-Gracia et al.<sup>[22]</sup> Briefly, the pDNA localizations were clustered using a mean shift algorithm with a bandwidth of 80 nm. An ellipse was fitted on the obtained clusters in order to filter out clusters with an aspect ratio higher than 5. Other filters are also applied: minimum 30 localizations per cluster, maximum 350 nm diameter for the longest axis and minimum 300 nm distance between the cluster density centers. As an output, we obtained the number of localizations in each pDNA cluster and the pBAE localizations within 3 times the cluster radius.

## Acknowledgements

Financial support from MINECO/FEDER (grant RTI2018-094734-B-C22) is acknowledged. The Agència de Gestió d'Ajuts Universitaris i de Recerca (AGAUR) from the Generalitat de Catalunya, for their support through grant SGR 2017 1559 is acknowledged. L.A. acknowledges financial support from Horizon2020 (ERC-StG-757397), and by the NWO through the VIDI Grant 192.028. The authors acknowledge Miguel Ángel Lázaro for his kind support in polymer synthesis.

## Conflict of Interest

The authors declare no conflict of interest.

**Keywords:** direct stochastic optical reconstruction microscopy (dSTORM) · poly( $\beta$ -aminoester) nanoparticles · nanoparticle stability · cell trafficking

- [1] D. A. Bölükbas, S. Meiners, *Nanomedicine* **2015**, *10* (21), 3203–3212, <https://doi.org/10.2217/nnm.15.155>.
- [2] D. Bobo, K. J. Robinson, J. Islam, K. J. Thurecht, S. R. Corrie, *Pharm. Res.* **2016**, *33* (10), 2373–2387, <https://doi.org/10.1007/s11095-016-1958-5>.
- [3] S. Mura, P. Couvreur, *Adv. Drug Delivery Rev.* **2012**, *64* (13), 1394–1416, <https://doi.org/10.1016/j.addr.2012.06.006>.
- [4] J. Nam, S. Son, K. S. Park, W. Zou, L. D. Shea, J. J. Moon, *Nat. Rev. Mater.* **2019**, *4* (6), 398–414, <https://doi.org/10.1038/s41578-019-0108-1>.
- [5] A. Banerji, P. G. Wickner, R. Saff, C. A. Stone, L. B. Robinson, A. A. Long, A. R. Wolfson, P. Williams, D. A. Khan, E. Phillips, K. G. Blumenthal, *J. Allergy Clin. Immunol.* **2020**, <https://doi.org/10.1016/j.jaip.2020.12.047>.
- [6] L. Milane, M. Amiji, *Drug Delivery Transl. Res.* **2021**, No. 0123456789, <https://doi.org/10.1007/s13346-021-00911-y>.
- [7] C. Fornaguera, M. Guerra-Rebollo, M. A. Lázaro, C. Castells-Sala, O. Meca-Cortés, V. Ramos-Pérez, A. Cascante, N. Rubio, J. Blanco, S. Borrós, *Adv. Healthcare Mater.* **2018**, <https://doi.org/10.1002/adhm.201800335>.
- [8] L. Ke, P. Cai, Y. Wu, X. Chen, *Adv. Ther.* **2020**, *3* (6), 1900213, <https://doi.org/10.1002/adtp.201900213>.
- [9] M. Foldvari, D. W. Chen, N. Nafissi, D. Calderon, L. Narsineni, A. Rafiee, *J. Controlled Release* **2015**, <https://doi.org/10.1016/j.jconrel.2015.12.012>.
- [10] N. Segovia, P. Dosta, A. Cascante, V. Ramos, S. Borrós, *Acta Biomater.* **2014**, *10* (5), 2147–2158, <https://doi.org/10.1016/j.actbio.2013.12.054>.
- [11] P. Dosta, N. Segovia, A. Cascante, V. Ramos, S. Borrós, *Acta Biomater.* **2015**, *20*, 82–93, <https://doi.org/10.1016/j.actbio.2015.03.029>.
- [12] X. Su, J. Fricke, D. G. Kavanagh, D. J. Irvine, *Mol. Pharm.* **2011**, *8* (3), 774–787, <https://doi.org/10.1021/mp100390w>.
- [13] C. A. Hong, A. A. Eltoukhy, H. Lee, R. Langer, D. G. Anderson, Y. S. Nam, *Angew. Chem. Int. Ed.* **2015**, *54* (23), 6740–6744, <https://doi.org/10.1002/anie.201412493>.

- [14] P. Brugada-Vilà, A. Cascante, M. A. Lázaro, C. Castells-Sala, C. Fornaguera, M. Rovira-Rigau, L. Albertazzi, S. Borros, C. Fillat, *Theranostics* **2020**, <https://doi.org/10.7150/thno.40902>.
- [15] P. Dosta, I. Tamargo, V. Ramos, S. Kumar, D. W. Kang, S. Borrós, H. Jo, *Adv. Healthcare Mater.* **2021**, *2001894*, 1–11, <https://doi.org/10.1002/adhm.202001894>.
- [16] R. Riera, N. Feiner-Gracia, C. Fornaguera, A. Cascante, S. Borrós, L. Albertazzi, *Nanoscale* **2019**, *11* (38), <https://doi.org/10.1039/c9nr02858g>.
- [17] S. Pujals, L. Albertazzi, *ACS Nano* **2019**, *13* (9), 9707–9712, <https://doi.org/10.1021/acsnano.9b05289>.
- [18] M. J. Rust, M. Bates, X. Zhuang, *Nat. Methods* **2006**, *3* (10), 793–795, <https://doi.org/10.1038/nmeth929>.
- [19] M. Bates, S. A. Jones, X. Zhuang, *Cold Spring Harb. Protoc.* **2013**, *8* (6), 498–520, <https://doi.org/10.1101/pdb.top075143>.
- [20] J. Xu, H. Ma, Y. Liu, *Curr. Protoc. Cytom.* **2017**, *81* (1).
- [21] C. Fornaguera, C. Castells-Sala, M. A. Lázaro, A. Cascante, S. Borrós, *Int. J. Pharm.* **2019**, *5* (569), 118612.
- [22] N. Feiner-Gracia, M. Beck, S. Pujals, S. Tosi, T. Mandal, C. Buske, M. Linden, L. Albertazzi, *Small* **2017**, *13* (41), 1701631.
- [23] S. Brunner, T. Sauer, S. Carotta, M. Cotten, M. Saltik, E. Wagner, *Gene Ther.* **2000**, *7*, 401–407.
- [24] D. A. Dead, D. D. Strong, W. E. Zimmer, *Gene Ther.* **2005**, *12*, 881–890.
- [25] A. P. Lam, D. A. Dean, *Gene Ther.* **2010**, *17*, 439–447.
- [26] J. D. Larsen, N. L. Ross, *Gene Med.* **2012**, *14*, 580–589.

---

Manuscript received: September 28, 2021  
Revised manuscript received: February 24, 2022  
Accepted manuscript online: February 25, 2022  
Version of record online: March 18, 2022